

---

## APPENDIX A: Solvent effect

---

The solvent effect has been used to describe the increased CV displacement of ions with respect to increasing humidity of carrier flow [1-3]. Simply, greater CV displacement is accomplished by manufacturing a larger difference between ion mobility in the high and low field regions of the applied asymmetric waveform by decreasing the mobility of the ion-molecule cluster by encouraging the solvation of water molecules. This solvation is likely only to occur in the low field region as the high field strength is too strong. The likelihood of solvation within the low field is dependent on the concentration of water molecules present. The on-set of the solvent effect for theoretical conditions are described within both Krylova *et al.* [1] and Eiceman and Kapras [2], it is replicated here.

Assuming a concentration of water molecules of 30 ppm, using the ideal gas law at room temperature and atmospheric pressure, there should be  $\sim 7.3 \times 10^{14}$  molecules/cm<sup>3</sup>. Additionally, the collision rate for successful interactions between the ion and neutrals is stated as  $\sim 1 \times 10^{-9}$  cm<sup>3</sup>/molecules·s [2]. The time between successful collisions of ions and water molecules will be the inverse of the product of these two quantities. For this particular example the time for an ion to interact with a water molecule is approximately 1.37  $\mu$ s. This time is then compared with the time of the low field region within each waveform, this then provides the likelihood that there is the capacity for larger ion molecular clusters to be formed before they are lost due to the commencement of the next high field region.

The results provided through this approach are a simplification and the time obtained between ion and water molecule interaction is less than the time of the low field region

does not necessarily prohibit the formation of such clusters as each individual ion undergoes unique and random interactions.

Shvartsburg questions the validity of the solvent effect as the reason for the observed behaviour. This is through his mathematical treatment (Equation A.1) which calculates there should be many more interactions with water molecules before the observed on-set [4].

$$\tau_v = \frac{1}{N\Omega c_v} \sqrt{\frac{\pi\mu}{8k_B T}} \quad \text{A.1}$$

Where  $\tau_v$  is the mean free time between ion and water vapour interaction,  $N$  is the number density of ions,  $\Omega$  is the cross section of the ions,  $k_B$  is the Boltzmann constant,  $T$  is the temperature,  $\mu$  is the reduced mass and  $c_v$  is the concentration of the water vapour.

Equation A.1 does not include a quantity describing the likelihood of a successful solvation following an interaction, which is included in the previous treatment. This may reconcile the difference of opinion.

An alternative treatment to assessing solvation is to consider the enthalpy and entropy, as discussed by Krylov and Eiceman [5]. Equation A.2 describes the average number of solvated molecules on to an ion.

$$n_{av} = \frac{C \exp((H/T) - S)}{1 - C \exp((H/T) - S)} \quad \text{A.2}$$

Where  $n_{av}$  is the average number of solvated molecules to the ion,  $C$  is the concentration of possibly solvating neutrals,  $H$  is the enthalpy and  $S$  is the entropy.

Assuming the enthalpy and entropy are constants of 5500 K and 14, applying Equation A.2 over a range of concentrations indicates that the onset of total solvation spreads over several orders of magnitude [5]. This suggests that any modification of the mobility experienced through clustering happens across a large range of concentrations as the average number of solvated ions within a swarm changes. It therefore appears that even with a high concentration it is unlikely that ions will experience greater levels of solvation with several clustered water molecules.

---

## APPENDIX B: Momentum transfer theory

---

The momentum transfer theory for use in describing ion behaviour within ion mobility studies is predominantly attributed to Mason and McDaniel [6, 7]. The theory presented here is based on their work. The outcome of this appendix is an expression that describes the velocity of ions; which is dependent upon the velocity of the different constituents and their properties.

The force on an ion following a collision with a neutral can be described by Newton's second law of motion. The force gained prior to the collision is equal to the momentum gained by the ion from the applied electric field per unit time. The momentum lost by an ion following an interaction is harder to understand as it depends upon the masses of the constituents, the angle at which they strike one another and the specific elasticity of the interaction given the orientation. To simplify the process an assumption is made. The momentum lost is taken to be the average momentum lost per collision, multiplied by the average number of collisions in unit time that produce the same average momentum lost and then summed over all possible collisions.

The relative momentum of an ion-molecule collision.

$$p = \mu v_r \tag{B.1}$$

Where  $p$  is the momentum,  $\mu$  is the reduced mass and  $v_r$  is the relative velocity.

Considering a single collision the momentum transferred to a gas molecule has a component parallel to  $v_r$ .

$$\delta(\mu v_r) = \mu v_r (1 - \cos \theta) \tag{B.2}$$

Where  $\theta$  is the relative deflection angle of the collision.

It is expected random components of the interaction average to zero leaving only the dependence on the drift velocity. The average momentum passed to the gas per collision.

$$\delta(\mu v_r) = \mu v_d (1 - \cos \theta) \quad \text{B.3}$$

The average number of collisions an ion makes per unit time that has an angle of deflection between  $\theta$  and  $\theta + d\theta$  [7].

$$N \bar{v}_r 2\pi \sigma(\theta, \bar{v}_r) \sin \theta d\theta \quad \text{B.4}$$

Where  $\sigma(\theta, \bar{v}_r)$  is the differential cross section for scattering through an angle  $\theta$  at velocity  $\bar{v}_r$ .

Combining Equations B.3 and B.4 and integrating over all deflection angles results in a new expression for the momentum loss.

$$\mu v_d N \bar{v}_r 2\pi \int_0^\pi (1 - \cos \theta) \sigma(\theta, \bar{v}_r) \sin \theta d\theta \quad \text{B.5}$$

To better handle Equation B.5 a diffusion cross section,  $\Omega_D$ , is defined.

$$\Omega_D(\bar{\mathcal{E}}) = 2\pi \int_0^\pi (1 - \cos \theta) \sigma(\theta, \bar{v}_r) \sin \theta d\theta \quad \text{B.6}$$

Where  $\bar{\mathcal{E}} = \frac{1}{2} \mu \bar{v}_r^{-2}$  is the mean relative energy of collisions.

The ion neutral collision frequency can also be defined.

$$\nu(\bar{\mathcal{E}}) = N \bar{v}_r \Omega_D(\bar{\mathcal{E}}) \quad \text{B.7}$$

Equation B.5 can now be expressed using these newly defined terms.

$$eE = \mu v_d \bar{v}(\mathcal{E}) \quad \text{B.8}$$

Where  $e$  is the fundamental charge.

Equation B.8 is useful as it is in terms of the drift velocity and therefore the mobility coefficient via Equation 1.1. A complication remains in that the average energy is in terms of the average relative velocity as required through Equation B.7.

There is a difference between the sum of averages and the average of a sum but as an approximation they can be related.

$$\overline{v_r^2} = \overline{(v+V)^2} = \overline{v^2} + \overline{V^2} \quad \text{B.9}$$

Where  $v$  is the velocity of the ions and  $V$  is the velocity of the gas molecules.

The velocity, and hence the kinetic energy, of the gas molecules is entirely due to thermal energy since they can not be affected by an applied electric field.

$$\frac{1}{2} M \overline{V^2} = \frac{3}{2} k_b T \quad \text{B.10}$$

At low enough electric field strengths the velocity of ions would also be predominantly attributable to the thermal environment. For high electric field strengths additional information is required which is found through considering energy balance.

For a strong enough electric field the motion of ions will predominantly be dependent upon the applied field and not any thermal component. Assuming this makes the thermal component of the ion velocity negligible it is tempting to consider the ion velocity as the drift velocity. However, this is not possible because any interaction of the ions with the

neutral carrier gas energy is absorbed and part of it is randomised. The ion velocity component,  $\bar{v}^2$ , is therefore observable as drift motion and also as an additional random component.

The average work done by the electric field on an ion per unit time is equal to the force imposed upon the ion, multiplied by the drift velocity. Equation B.11 describes the average energy gained from the field per unit time.

$$\varepsilon = eE v_d \quad \text{B.11}$$

The average energy lost per collision is the initial energy minus the resultant energy of averaged velocities.

$$\varepsilon = \frac{1}{2} m \bar{v}^2 - \frac{1}{2} m \bar{v}'^2 \quad \text{B.12}$$

Where  $\bar{v}'$  is the average ion velocity after collision.

Multiplying Equation B.12 by the collision frequency, as defined by Equation B.7, provides an expression that is equivalent to Equation B.11. The result can be expressed as an energy balance.

$$\varepsilon = \frac{1}{2} m \left( \bar{v}^2 - \bar{v}'^2 \right) \nu(\varepsilon) = eE v_d \quad \text{B.13}$$

The full derivation of describing the velocity and energy of the ions after collision by considering only the velocities of the ions and gas molecules before collision requires further manipulation. The conservation of energy and momentum is explored while also operating within centre of mass co-ordinates. The complete derivation is not replicated here but is available from Mason and McDaniel [7].

It is now possible to create an expression dependent on  $v$  and  $V$  and not  $v'$ .

$$eEv_d = \frac{mM}{(m+M)^2} (mv^{-2} - M\bar{V}^{-2}) v(\bar{\mathcal{E}}) \quad \text{B.14}$$

To find a relationship only in terms of the masses and velocities Equation B.8 and B.14 are rearranged to equal  $eE/v(\bar{\mathcal{E}})$  and set equal to one another. After some re-arrangement, and placing the terms in terms of kinetic energy, Equation B.15 is obtained.

$$\frac{1}{2}mv^{-2} = \frac{1}{2}M\bar{V}^{-2} + \frac{1}{2}mv_d^2 + \frac{1}{2}Mv_d^2 \quad \text{B.15}$$

---

## APPENDIX C: Drift velocity

---

Alternatively to Appendix B the drift can be expressed as dependent upon the electric field strength and a reduced mass. This reduced mass is dependent on the mass of the ions and neutral constituents and describes how energy is shared following an interaction. Assuming constant acceleration between ion-molecule interactions the drift velocity can be described.

$$v_d = \left(1 + \frac{m}{M}\right) \frac{eE}{m} \tau = \frac{eE}{\mu} \tau \quad \text{C.1}$$

Where  $\tau$  is the mean free time between collisions and  $\mu$  is the reduced mass.

Equation C.1 comes from Newton's second law of motion and the expression for velocity given constant acceleration.

$$v = at + u \quad \text{C.2}$$

Where  $t$  is the time the acceleration acts over and  $u$  is the initial velocity. Assuming all ion kinetic energy is lost when a collision occurs the initial velocity is equal to zero.

The force applied to the ion is the Lorentz force with no magnetic field contribution, previously introduced in Chapter 1.

$$F = eE \quad 1.2$$

The reduced mass expression is obtained from a consideration of the interaction of an ion and gas molecule and Newton's second and third laws of motion. The interaction between an ion and gas molecule are considered since it is assumed there are many more gas molecules than ions within the separation region and therefore only the velocity of the ions is of concern.

Force of ion at interaction.

$$F_{m-M} = ma_m \quad \text{C.3}$$

Where  $m$  is the mass of the ion.

Force of molecule at interaction.

$$F_{M-m} = Ma_M \quad \text{C.4}$$

Where  $M$  is the mass of the gas molecule.

As described by Newton's third law of motion, the forces are equal but opposite.

$$F_{m-M} = -F_{M-m} \quad \text{C.5}$$

$$ma_m = -Ma_M \quad \text{C.6}$$

The relative acceleration between the two bodies can then be found.

$$a = a_m - a_M = \left(1 + \frac{m}{M}\right)a_m. \quad \text{C.7}$$

Combining Equations C.2, 1.2 and C.7 we arrive with Equation C.1.

---

## APPENDIX D: Energy resulting from interactions of ions and neutrals

---

Through the application of an asymmetric waveform and the presence of neutrals there are means for increasing and decreasing the energy that the ion experiences. It is useful to understand which parameters and properties directly affect the energy which the ion experiences. The following treatment is taken from Nazarov *et al.* [8] with additional derivation undertaken independently.

It is assumed that any energy gained by an ion due to the electric field it experiences is dissipated following an interaction with the neutral carrier gas. The energy an ion experiences is therefore dependent upon the electric field strength and neutral number density. The energy gained by an ion within the separation region between collisions.

$$\Delta\varepsilon_i = eE\lambda = \frac{eE}{\Omega N} = k_b T \frac{eE}{\Omega P} \quad \text{D.1}$$

Where  $\Delta\varepsilon$  is the change in energy,  $e$  is the fundamental charge,  $E$  is the strength of the electric field,  $\lambda$  is the mean free path,  $\Omega$  is the effective cross sectional area,  $N$  is the molecular number density within the separation region,  $k_b$  is the Boltzmann constant,  $T$  is the temperature and  $P$  is the pressure.

The equation is derived from the general expression for work done,  $\varepsilon = F \cdot s$ , where the work done is equal to the force required multiplied by the displacement ( $s$ ) it acts over. The equation assumes constant electric field strength between collisions.

The mean free path ( $\lambda$ ) is the displacement between interactions and can be approximated (as in equation D.1).

$$\lambda \approx \frac{1}{N\Omega} \quad \text{D.2}$$

The energy acquired by the ions is also equivalent to the summation from three sources, the gas temperature, ion kinetic energy and neutral molecule kinetic energy.

$$\varepsilon_i = \frac{mv_i^2}{2} = \frac{mv_d^2}{2} + \frac{Mv_d^2}{2} + \frac{3k_bT}{2} \quad \text{D.3}$$

Where  $\varepsilon_i$  is the energy of the ions,  $v_i$  is the velocity of the ions,  $m$  is the mass of the ions,  $v_d$  is the drift velocity and  $M$  is the mass of the neutral molecules.

The separation of acquired ion energy between the constituents of the medium depends on the ion mass,  $m$ , and mass of molecules in the supporting atmosphere,  $M$ . When molecules and ions have similar masses the energy is equally distributed between the ions and molecules. For heavy ions,  $m \gg M$ , the energy gained from the electric field remains principally in ion motion. In the case of light ions the situation is reversed and any acquired energy principally results in increased kinetic energy of the gas molecules. The ion motion is sometimes described as the result of drift movement owing to the applied field and random movement resulting from ion collisions with the neutral supporting atmosphere.

---

## APPENDIX E: Pressure and ion motion within separation region

---

Through the ratio  $E/N$  the pressure of the carrier flow within a FAIMS device affects ion motion. This appendix considers the effect of a changing pressure with respect to the longitudinal and transverse ion motion (as defined in Figure 2.1).

### E.I Pressure effects on longitudinal ion motion

To assess the effects of changing pressure on the longitudinal motion of ions within a separation region it is useful to consider two scenarios and compare them against one another. The ideal gas law for a unit volume.

$$P = Nk_bT \quad \text{E.1}$$

Where  $P$  is the pressure and  $N$  is the molecular gas density. Note that this expression is only dependent upon fundamental constants and experimentally quantifiable quantities.

Two separate scenarios can therefore be described.

$$\text{Scenario 1} \quad N_1 = \frac{P_1}{k_bT} \quad \text{E.2}$$

$$\text{Scenario 2} \quad N_2 = \frac{P_2}{k_bT} \quad \text{E.3}$$

The molecular gas density's and pressures between the two scenarios are currently completely independent of one another but imposing the condition that the two scenarios have the same flow rate enables some relations to be determined.

Condition of constant flow.

$$f_s = \frac{\Delta N}{\Delta t} \quad \text{E.4}$$

When  $f_s$  is the flow through the separation region,  $\Delta t$  can be considered the residence time ( $t_{res}$ ).

Since the flows of the two considered scenarios are equivalent, and  $N$  is dependent on  $P$  through Equation E.1.

$$\frac{N_1}{t_{res,1}} = \frac{N_2}{t_{res,2}} \quad \text{E.5}$$

$$t_{res,2} = \left( \frac{N_2}{N_1} \right) t_{res,1} \quad \text{E.6}$$

$$t_{res,2} = \left( \frac{P_2}{P_1} \right) t_{res,1} \quad \text{E.7}$$

Taking the ion longitudinal velocity ( $v_{||}$ ) to be  $v_{||} = l/t_{res}$ .

$$v_{||,2} = \left( \frac{N_1}{N_2} \right) v_{||,1} \quad \text{E.8}$$

$$\frac{v_{||,2}}{v_{||,1}} = \frac{N_1}{N_2} \quad \text{E.9}$$

It is now the case that ion velocity is inversely proportional to gas density so less material in the separation region leads to a shorter residence time of ions, and vice versa.

## E.II Pressure effects on transverse ion motion

To assess the effect of changing the pressure within the separation region on the transverse motion of ions the same method will be employed as for assessing the longitudinal motion of ions.

Only ions with a displacement smaller than the effective gap height of the separation will go on to be detected.

$$\text{Scenario 1} \quad v_{\perp 1} = \frac{g_{eff}}{t_{res,1}} = \frac{\beta \Delta K_1}{T} \quad \text{E.10}$$

$$\text{Scenario 2} \quad v_{\perp 2} = \frac{g_{eff}}{t_{res,2}} = \frac{\beta \Delta K_2}{T} \quad \text{E.11}$$

Once again, setting the total flow through the separation region equal in both scenarios as described by Equation E.4. The residence times are still described by Equations E.6 and E.7 since these quantities are independent of the applied asymmetric waveform as described by Equation 2.32.

$$v_{\perp 1} = \left( \frac{P_1}{P_2} \right) v_{\perp 2} \quad \text{E.12}$$

Which is the same result as for the longitudinal ion motion case.

---

## APPENDIX F: Waveforms

---

The fundamental difference between traditional IMS devices and the later FAIMS technology is the electronic waveform applied and how it is utilised. Within this appendix the properties required of a waveform, ideal and practical, employed by FAIMS systems will be discussed. Much of what is presented here is derived from work by Shvartsburg [4, 9].

### F.I Suitable waveform

The waveform used in a FAIMS instrument needs to separate ions due to the change in mobility of ions between high and low field regions. To ensure that any difference observed is due to the unique properties of ions within a swarm it is required that the electric field implemented does not result in a net force upon the ions within the separation region.

To define the design of electronic waveforms which would satisfy the above requirement the mobility coefficient, which can be considered as a sum of a field independent and a field dependent part, is first considered. The field dependent part is assessed as a deviation from an arbitrary field value,  $E_F$ .

$$K(E) = K_F [1 + fn(E - E_F)] \quad \text{F.1}$$

Where  $fn$  denotes a function and  $K_f$  is the mobility coefficient at  $E_f$ . In Chapter 2  $fn$  was referred to as the  $\alpha$  function.

Remembering that drift velocity, and hence the displacement, is attributable to the action of an electric field Equation F.1 can be broken down into field dependent and independent parts.

$$d(t) = \int_0^t K(E)E(t)dt = K_F \int_0^t E(t)dt + K_F \int_0^t fn[E(t) - E_F]E_t dt \quad \text{F.2}$$

The waveform of the electric field as a function of time ( $E(t)$ ) can be described by the product of an amplitude and a time dependent function.

$$E(t) = E_{\max} F(t) \quad \text{F.3}$$

Where  $E_{\max}$  is the maximum value of  $E(t)$  and  $F(t)$  is a time dependent function representative of  $E(t)$ .

For a difference of coefficients of mobility to arise due only to the identity of the ions within an ion swarm the waveform applied has to be of a certain form. At a time  $t_c$ , the first but not the second term on the right hand side of equation F.2 must cancel.

With regard to the first term having to cancel this is graphically equivalent to the areas between the waveform and the time axis for the positive and negative polarities being equal to one another. If this condition is met it means that the net forcing due to the electric field over a waveform period in each polarity equals zero.

$$\int_0^{t_c} F(t)dt = 0 \quad \text{F.4}$$

The requirement that the second term on the right hand side of equation F.2 does not cancel is the result that the waveform must be asymmetric. This ensures that an ions average mobility coefficient is not equal in each of the polarities of the waveform. If this were the case there would be no separation of ions due to the ion species unique mobility coefficients. The action of the positive and negative parts of the waveform would result in a net zero displacement for all ions.

With these constraints firmly in place suitable waveforms can be investigated.

In equation F.3 the waveform was split into a constant value and a time dependent function. To satisfy the criteria for a suitable waveform only the time dependent function is considered; the general form of which is presented below.

$$\langle F_k \rangle = \frac{1}{t_c} \int_0^{t_c} F^k(t) dt \quad \text{F.5}$$

The  $\langle \rangle$  brackets denote an average and  $k$  is the function order.

With this expression different orders are considered. For  $k = 1$  the first expression on the right hand side of Equation F.2 cancels when  $F_+(t) = -F_-(t + const)$ , unfortunately so does the second term on the right hand side of the same expression. This waveform has failed the criteria required.

Now considering  $k = 2$ . This requires squaring the waveform which results in the entire waveform becoming positive. It then becomes impossible for the effect of the electric field to cancel itself over a period of the waveform, which will result in net forcing on the ions. This again fails the criteria required and would occur for any even value of  $k$ .

All even values of  $k$  and  $k = 1$  are excluded. Now considering  $k = 3$  the first term of Equation F.1 on the right hand side will equal zero as the function has not been squared and the time dependent second term will not average to zero. The first  $k$  value that satisfies the conditions required has been found. In fact all odd terms greater than  $k = 1$  satisfy the conditions set. The general expression can now be written.

$$\langle F_{2k+1} \rangle = \frac{1}{t_c} \int_0^t F^{2k+1}(t) dt \neq 0 \quad \text{F.6}$$

## F.II Practical waveforms

An idealised waveform often used to illustrate how ions are separated in a FAIMS device is constructed from a high field region for a time  $t_1$  and a low field region in the opposite polarity for a time  $t_2$  where  $t_1 < t_2$ . The regions are intentionally constrained by  $|E_{\max}|t_1 = |E_{\min}|t_2$ . A diagram of this ideal waveform is shown in Figure 1.6.

Not only does this waveform satisfy the conditions previously set down in section F.I but it also provides a constant electric field environment within each polarity for the maximum amount of time. This uniformity maximises the time that forces acting on the constituents between the device electrodes are constant. Furthermore, maximising the time the extremes of field strength are experienced increases differences in mobility and the likelihood of clustering and de-clustering of ion-molecules, which is a recognised mechanism for species separation.

Waveforms within real systems aspire to this ideal but due to the practicalities of implementation (*i.e.* required period, limitations on circuitry complexity and power) a

concession is normally necessary. Figure F.1 is a real waveform as applied within an Owlstone FAIMS sensor.

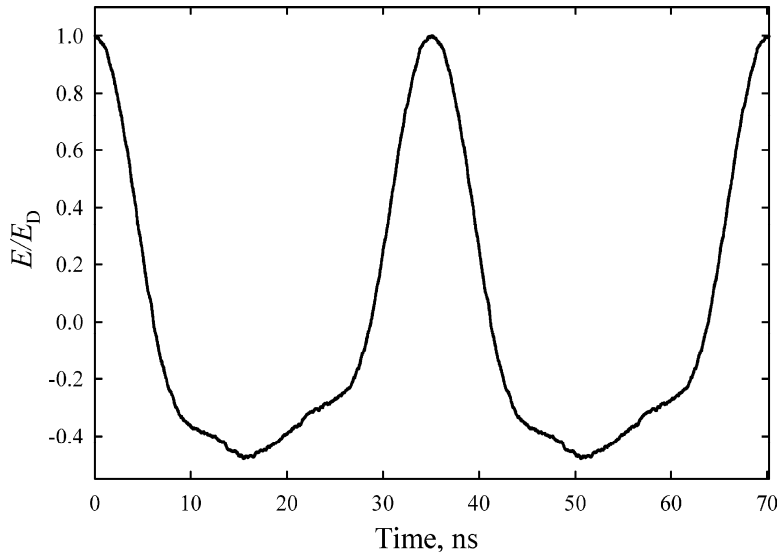


**Figure F.1** Waveform profile utilised by an Owlstone FAIMS sensor, normalised to the maximum amplitude of the dispersion field (referred to here as  $E_D$ ) Originally from Schvartsburg *et al.*[9].

$\langle F_3 \rangle = 0.108$  and  $\langle F_5 \rangle = 0.105$ , stated as near optimum for many ions.

$\langle F_2 \rangle = 0.244$ , this value is 0.278 for Ionalytics and Thermo Fisher systems. This leads to less diffusional broadening.

The amplitude of ion oscillations has been described [9].

$$\Delta y = K(0)E_D \tau_c \Delta_f \quad \text{F.7}$$

Where  $\tau_c$  is the period of  $E(t)$  and  $\Delta_f$  characterises the waveform profile.  $\Delta_f = 0.214$  for Owlstone and 0.234 for Ionalytics and Thermo Fisher systems.

The amplitude in the high field segment of the Owlstone practical waveform is variable up to a maximum of 214 V. This corresponds to an  $E_D$  of 61 kV/cm. Within ambient conditions this corresponds to an  $E_D / N$  of 250 Td. From the Paschen curve for  $N_2$  the

---

breakdown threshold is  $\sim 700$  Td so the maximum field does not result in breakdown of the carrier gas.

For good ion transmission  $\Delta y \ll g$ . To minimise  $\Delta y$  the frequency, which is the inverse of  $\tau_c$ , can be increased. The greatest  $K(0)$  known for an ion in ambient air or  $N_2$  is  $\sim 3$   $\text{cm}^2/\text{V}\cdot\text{s}$ . Owlstone employs a frequency of 28.5 MHz (the highest frequency in IMS or MS) which will enable all ions to be detected. Smaller ions at higher  $E_D$  will not be suited to the high frequency.

The compensation field is created by bias amplifiers and superimposed on the waveform. They have a range of  $\pm 11$  V. This translates to a range of  $\pm 3$  kV/cm for  $E_c$  or  $\pm 13$  Td for  $E_c / N$  which suffices for all ions explored so far at any  $E_D$  [9].

---

## APPENDIX G:Modelling permeation rates from permeation sources

---

There are several ways of approaching a theoretical model for permeability of analyte through a permeation source. Models that were investigated included those based upon obstruction effects, hydrodynamics, free volume theory and effusion. To be as general as possible a general rule was taken as the basis for the modelling, based on Fick's first law of diffusion.

$$Flux = -P_p A(c_2 - c_1) \quad G.1$$

Where  $P_p$  is the permeability coefficient,  $A$  is the surface area through which permeation can occur and  $c$  is the concentration of analyte between regions 1 and 2 with movement of material from region 1 to 2. A labelled schematic of a permeation source is shown in

Figure G.1.

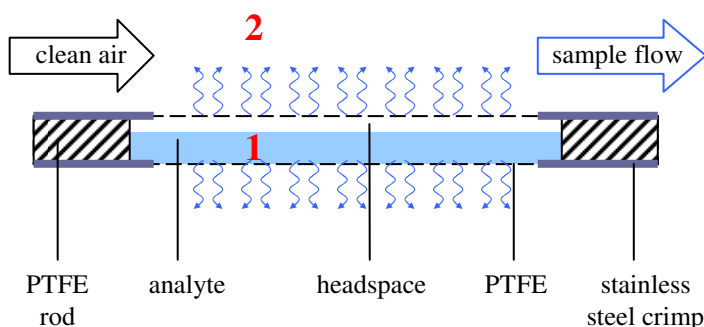


**Figure G.1** Schematic of permeation source

Factors that were treated as affecting the permeation rate were:

- thickness of the permeation source walls
- temperature
- pressure difference across the permeable barrier
- interaction of permeating material with permeable surface

From Equation G.1, using permeation sources with identical dimensions, the effect due to the thickness of the walls will be contained within the permeability coefficient. Therefore, it is assumed that the permeability coefficient ( $P_p$ ) represents a collection of parameters that are deemed constant or assumed constant for the purposes of the modelling. This is a potential source of error due to variations in dimensions through manufacture.

Permeation rate is considered dependent upon temperature through two mechanisms. The concentration gradient will be dependent upon the vapour pressure of analyte within the gaseous phase within the permeation source. As the ambient temperature increases so will the concentration within the gas phase and the concentration gradient will increase, increasing the permeation rate. The increase of permeated analyte with respect to temperature through this mechanism is linear and, by a rule of thumb, that permeation through a permeation source doubles with every increase of 10 °C.

Non-linear increase of permeation rate with respect to temperature is attributable to the change in solubility of the analyte with the PTFE, even the expansion of the polymer may allow more pathways for the analyte to escape. This behaviour is not explicitly dealt with within Equation G.1 and therefore falls within the permeability coefficient.

It is proposed that the main method for permeation through the permeation source walls is movement through voids within the PTFE structure.

Since there are several temperature effects an involved model requires extensive experimentation to obtain the required data. This may be worth while if the permeation of a single compound was required in great detail but for most cases a ‘ball park figure’ is adequate to first set-up apparatus around the correct permeation rate and then confirm the

amount of permeation that is liberated through gravimetric means. Obtaining the permeation of a source over a few temperatures is likely to be easier to acquire and more accurate than the discovery of particular temperature solubility dependencies.

Within this thesis it was not required for an in depth understanding of the permeation of analyte from any permeation source. It was typically acceptable to choose a temperature with respect to the previously mentioned 'rule of thumb' and tailor an exact analyte concentration through the management of experimental flows. For this reason, beyond some preliminary investigation, the modelling of permeation rates from permeation sources was not taken further.

---

# APPENDIX H: Tracking peaks

---

Peak fitting (as detailed in Chapter 4) was discussed in relation to how it can be used to track the evolution of ion responses. This Appendix describes how peak fitting was used to gain a fuller understanding of the data from experiments undertaken with an exponential dilution flask (EDF).

## H.I Situation

An EDF is used to generate a range of analyte concentrations. An attached instrument monitoring the contents of the EDF would first sample an initial concentration of analyte, which is then continuously diluted. The profile of the analyte concentration within the EDF is that of an exponential decrease. The initial sample concentration is often created by an injection of liquid analyte into the heated flask. It is important that the temperature of the flask is such as to ensure that the injected analyte volatilises quickly for assumptions in the theory to hold.

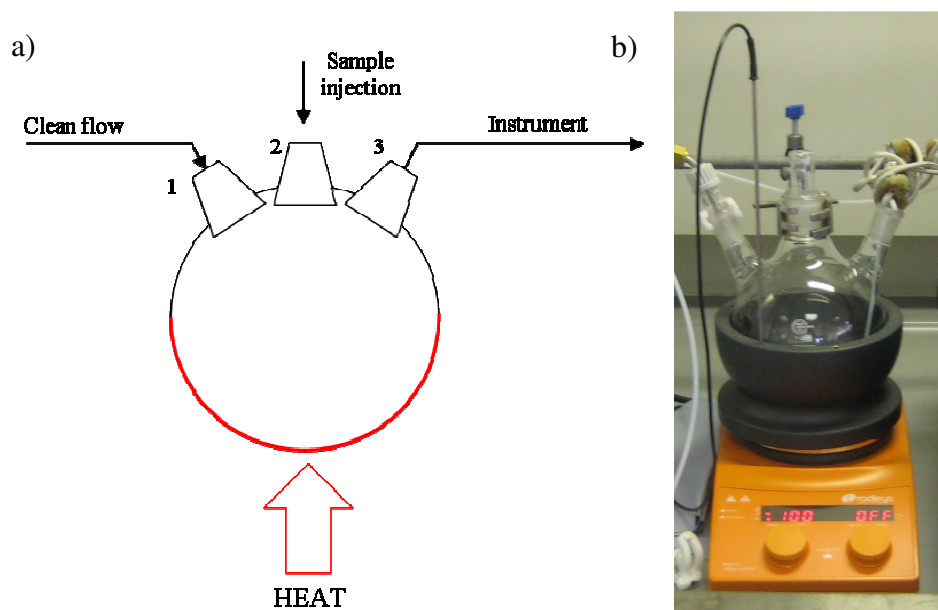


**Figure H.1** a) A schematic of an EDF set-up including the flows required for operation, b) photograph of EDF, (bulb diameter of 12.4 cm) used in experimentation, being heated.

The concentration of analyte present within the dilution flask can be calculated from experimental parameters.

$$c = c_0 \exp\left(\frac{-ut}{V_m}\right) \quad \text{H.1}$$

Where  $c$  is the concentration at time  $t$ ,  $c_0$  is the initial concentration at the time of injection,  $u$  is the flow rate of the clean flow into the dilution flask,  $t$  is the time since analyte injection and  $V_m$  is the volume of the dilution flask.

For each compensation voltage (CV) sweep individual peaks will be fitted to the data. It is of analytical interest to track an individual peak through time to determine a property such as the limit of detection. Peak fitting not only records the data points required to later plot the fitted peaks but also important properties of the fitted peak such as its CV position and maximum response. CV position of an ion response within FAIMS is recognised as being dependent upon the identity of the ion species that are responsible for the ion signal. It is therefore possible to isolate the response of a single ion species by only considering the data from fitted peaks that exist within a defined range (window) of CV.

## H.II Worked example

To demonstrate the isolation of signal, some example data will undergo the steps required to track the ion response believed to be associated with an analyte. The sample data is composed of 1,500 individual CV scans collected during an EDF experiment. Three peaks are fitted within each sweep. The maximum ion intensity of each fitted peak is displayed within Figure H.2 and the associated CV position of the maximum of each peak is displayed within Figure H.3.

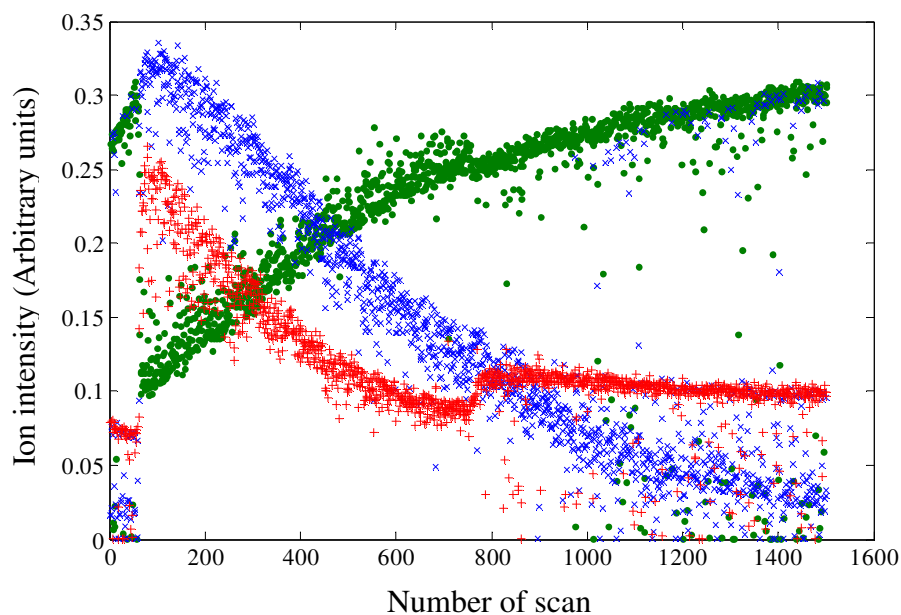


**Figure H.2** The ion intensities of fitted peaks displayed in CV order. Highest CV value (red +), medium CV value (blue x) and lowest CV value (green o).

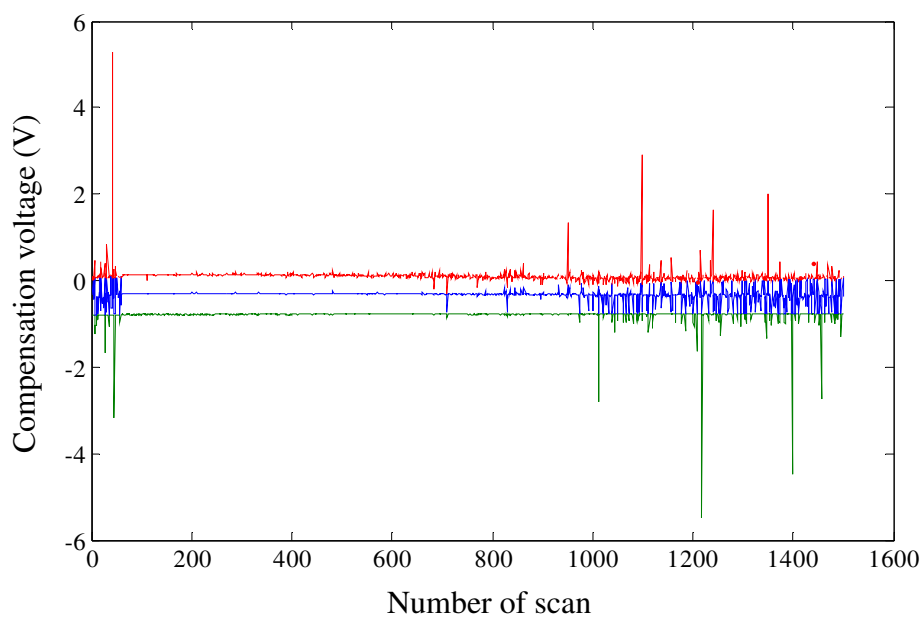


**Figure H.3** The CV position of the maximum of the fitted peaks described in Figure H.2

From Figure H.2 and Figure H.3 the peak fitting procedure is not perfectly consistent and has resulted in some potentially erroneous readings. For instance, from Figure H.2, beyond scan number 1,000, although there appears to be trends within the data, fits are

occasionally made interchangeably between ion species. To obtain more information from the data further isolation must occur.

### H.III Isolating desired data

In the case of an EDF experiment the signal-to-noise ratio (S/N) of an analyte response will continuously decrease. It therefore becomes more and more likely that peak fitting will fail. A procedure has been created to militate against this and provide a mathematical expression for the reduction in analyte signal. To help explain, the second fitted peak from the example data, initially displayed in Figure H.2, has been provided. The result is shown in Figure H.4.

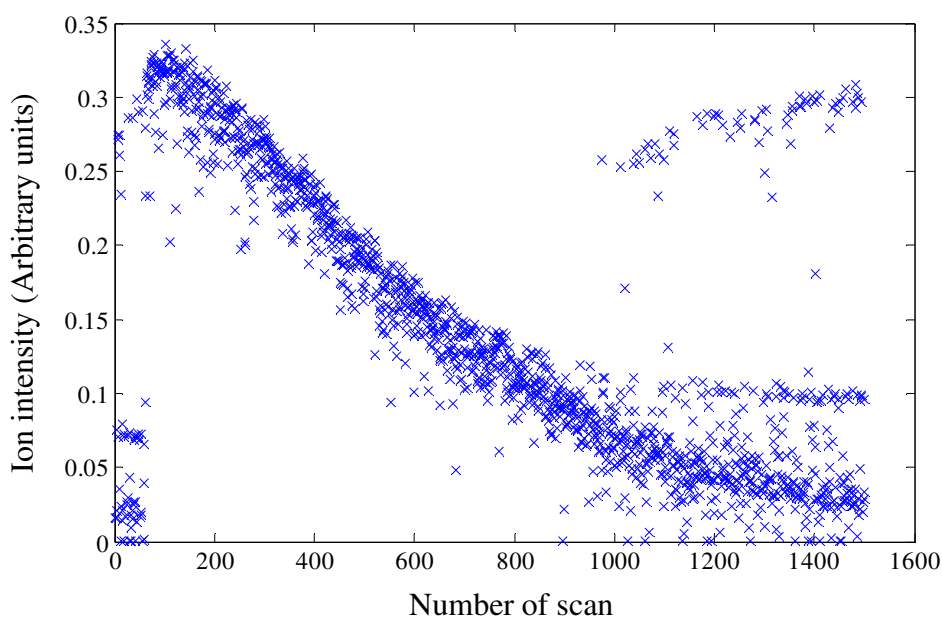


**Figure H.4** Fitted maximum peak intensity of the second fitted peak from 1500 CV scans during an EDF experiment.

Figure H.4 initially shows a fluctuating peak fit (0 - 50 scans). After the injection of the analyte (~ scan 50) a much more consistent and decreasing signal is in evidence. Later again, when the ion intensity becomes similar to the ion intensity seen before the analyte injection, the peak fit increasingly fluctuates.

As well as the maximum ion intensity the CV position of the fitted peak is also available over the same range. This information is shown in Figure H.5.

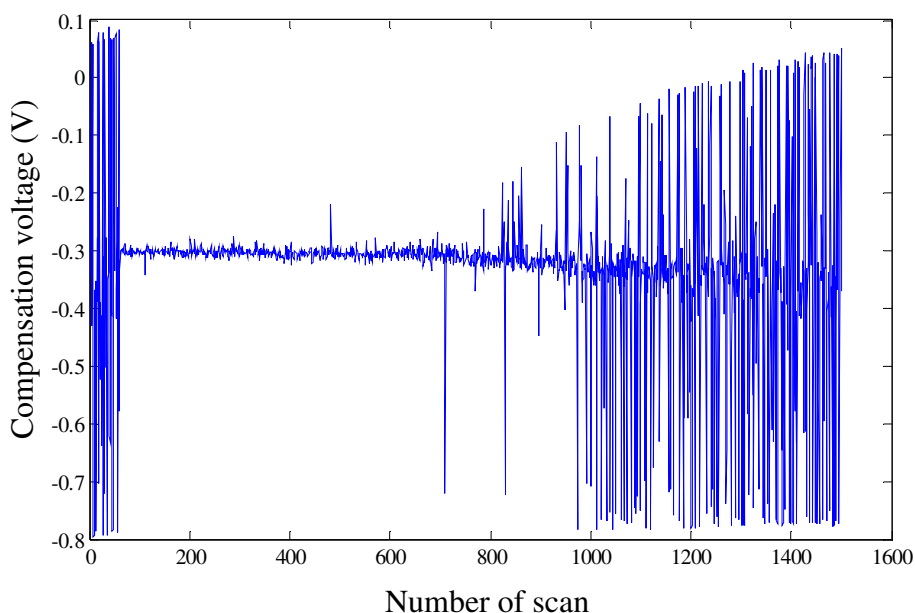


**Figure H.5** CV positions of the maximum of the second fitted peak from 1500 CV scans during an EDF experiment.

The data depicted in Figure H.5 closely matches the situation described by the ion intensities in Figure H.4. Initially, the signal fluctuates but then with the introduction of analyte the fitted peak stabilises until later, where the signal again fluctuates.

Since it is clear there is a relationship between the stability of the CV position and the introduction of the analyte it is reasonable to assume that the recorded CV position is representative of the ion species created by the addition of the analyte. It should be possible to filter out a good deal of incorrectly fitted data by only considering data that has a CV position similar to that where the signal is stable.

To specify the CV position range that data will be accepted two user inputs are required. The first input required is the range of scan numbers that best describes the CV position that is to be observed. The mean of this range is calculated. The second required user input

defines the standard deviation beyond the mean which provides a maximum and minimum CV value which data must possess to be considered further. The magnitude of the standard deviation is left as a user defined input since the output of the peak fitting procedure is dependent on several variables (number of detected ion responses, S/N, CV separation between ion responses, etc) and the ability to control this setting allows for management of complex results.

A line depicting the mean CV position and maximum and minimum CV values within a defined range is shown in Figure H.6. The resultant ion intensity data which only includes the data points which lie within the specified standard deviation of the mean is shown in Figure H.7.

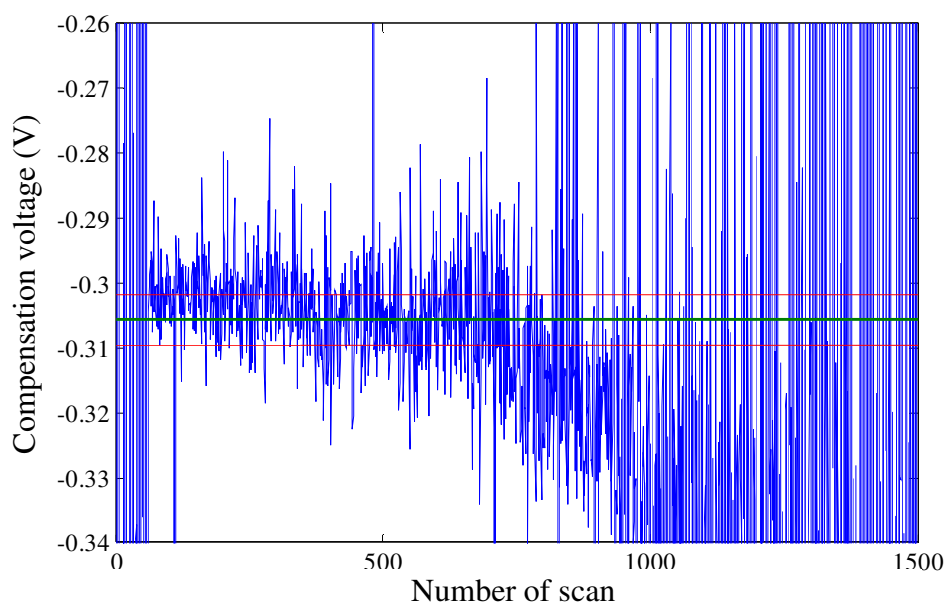


**Figure H.6** This is the data as depicted within Figure H.5 with the addition of the mean CV value in the Number of Scan range 200 - 800 (green) and the maximum and minimum limits (red). The limits in this example correspond to plus and minus 0.2 standard deviations from the mean as calculated from the same Number of Scan range.

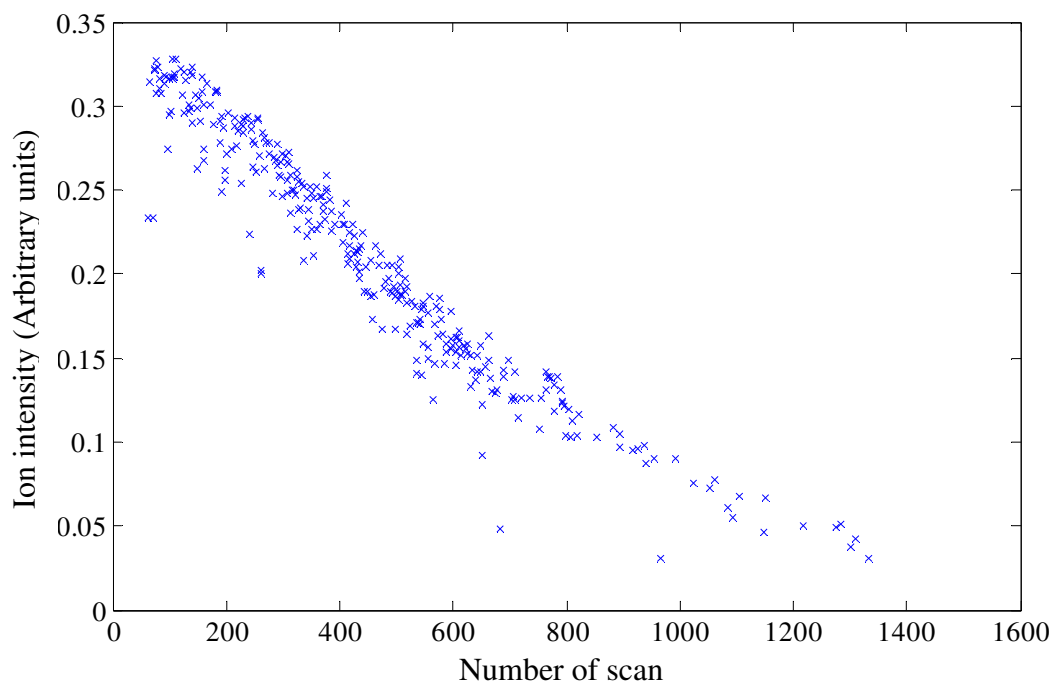


**Figure H.7** This is the same data as in Figure H.4 except only the data that corresponds to a CV position within the limits depicted within Figure H.6 are shown.

Now that the data has been filtered to only the points which are believed to be most representative of the analyte under study a curve can be fitted to the remaining data in the set. Since the experiment under study is an exponential dilution it is assumed that the form of the curve will be an exponential decrease. However, to fit a continuous curve there cannot be gaps within the data set. It is therefore necessary to fill the gaps created by isolating the relevant CV positioned data. This is accomplished by averaging the data points that are present either side of a missing data point and placing it in series.

#### **H.IV Creating replacements for missing data**

The replacement of missing data is required to allow a polyfit to be fitted to the data set. Any synthetic data should be representative of the raw data and not affect the resultant fit by their presence. Unfortunately, any methodology can introduce some bias within the data

set so an understanding of what occurs with the change of any settings is required to correctly appreciate the result.

The method employed in tracking peaks within this work is a moving array of calculated length. Every data point which has previously been disregarded (null result) due to the associated CV value being beyond the limit must be replaced. The moving array is populated by the values either side of the null result and the mean of the moving array is calculated. The mean value of the moving array then replaces the previously null result. The methodology is based upon the nearest neighbour Kernel methodology [10].

A brief example of how the moving array works is depicted in Table H.1. The second and third rows show the values that will be averaged for term numbers 100 and 102 respectively. The moving average size in the example is ten.

**Table H.1** Selection of filtered data from example data set.

Term Number	90	91	92	93	94	95	96	97	98	99	100	101	102	103	104	105	106	107	108	109	110	111	112	113	114	115
CV filtered data	0.32	0.31	NaN	0.32	NaN	NaN	0.27	NaN	NaN	0.29	NaN	0.32	NaN	0.3	0.32	0.32	0.33	0.32	NaN	0.32	NaN	NaN	0.33	NaN	NaN	NaN
Moving array for term 100	0.32	0.31		0.32			0.27			0.29	???	0.32		0.3	0.32	0.32	0.33	0.32		0.32						
Moving array for term 102				0.32			0.27			0.29		0.32	???	0.3	0.32	0.32	0.33	0.32								0.33

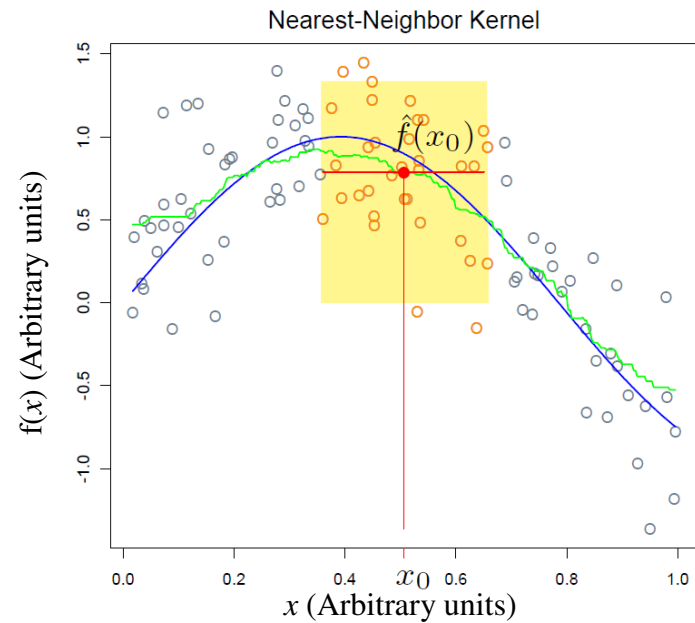


**Figure H.8** The green trace is a result of a thirty point nearest neighbour running mean smoother. Originally taken from Elements of Statistical Learning [10]

Care must be taken to reduce any artificial effects this procedure may introduce. Taking the mean is a reasonable average compared to the mode and median as it results in a new value being constructed as opposed to replication of an existing value from a different location. The range over which the mean is calculated should, however, be as small as possible. This is because increasing the array means that points further from the point to be replaced will have a contribution. Since the attempt is to artificially alter the data set as little as possible replacement points should be as locally relevant as possible.

The length of the moving array is calculated as the largest number of consecutive null results within the defined CV range used to specify what data was to be filtered. This is the minimum size of the moving array which provides a replacement for every null result.

The result of replacing the null results with the means provided from the moving array is shown in Figure H.9.

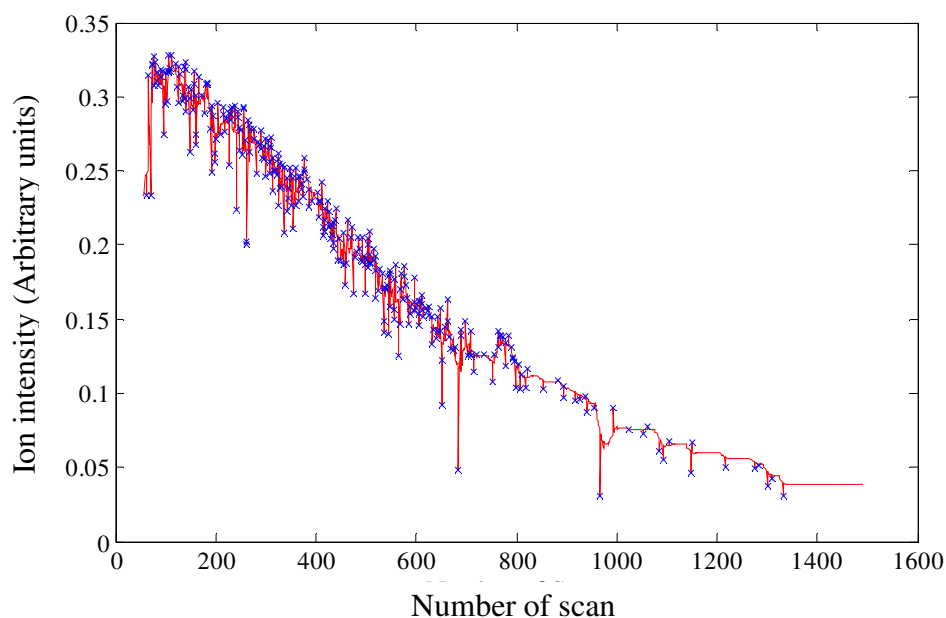


**Figure H.9** The filtered data (blue crosses) are shown alongside the replacement data as found through use of a moving array (red line connecting points).

There is now a total data set of the example data which is representative of only the points which correspond to the CV range dictated by the user.

## H.V Curve fit and extraction of equation

With the completed data set it is now possible to discover a line of best fit that describes the exponential decrease of ion intensity.

The natural logarithm of the amended data is taken. The result should be a linear decrease if the data set truly describes an exponential loss of signal. A linear regression is carried out over the defined range introduced within Section H.III and the constants describing the y-axis intercept and gradient of the linear line also describe the constants associated with the exponential decrease of the original amended data. This information is presented within Figure H.10.

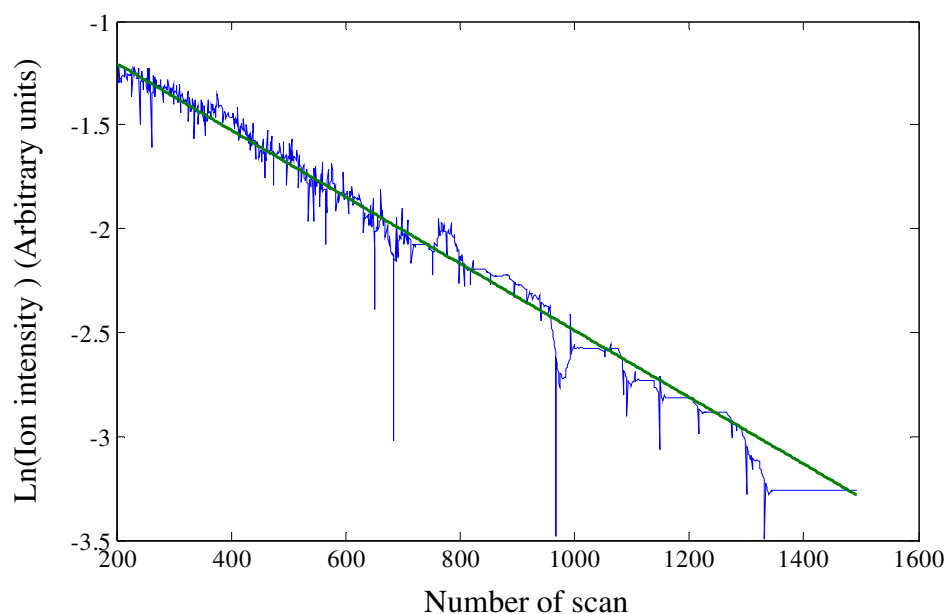


**Figure H.10** The natural logarithm of the amended data (blue line) and the line of best fit as calculated through a linear regression with respect to a user defined range (green line).

The equation of the line of best fit is described by Equation H.2 and the constants  $m$  and  $c$  can be used to construct an equation which describes the exponential decrease, Equation H.3.

$$y_l = mx + c \quad \text{H.2}$$

$$y_e = \exp(c) \times \exp(mx) \quad \text{H.3}$$

Where  $y_l$  are the  $y$  values of the linear line and  $y_e$  are the  $y$  values of the exponential decrease.

The results of the steps taken are shown below in Figure H.11. It appears that from variable data an acceptable exponential decrease has been fitted. However, this plot does not describe clearly the region that the fitted exponential is relevant. As noted, when considering the CV range to be defined within Section H.III, before and for a time after injection, the peak fitting fluctuates a great deal. This was hypothesised as being due to a lack of analyte ion response (low S/N).

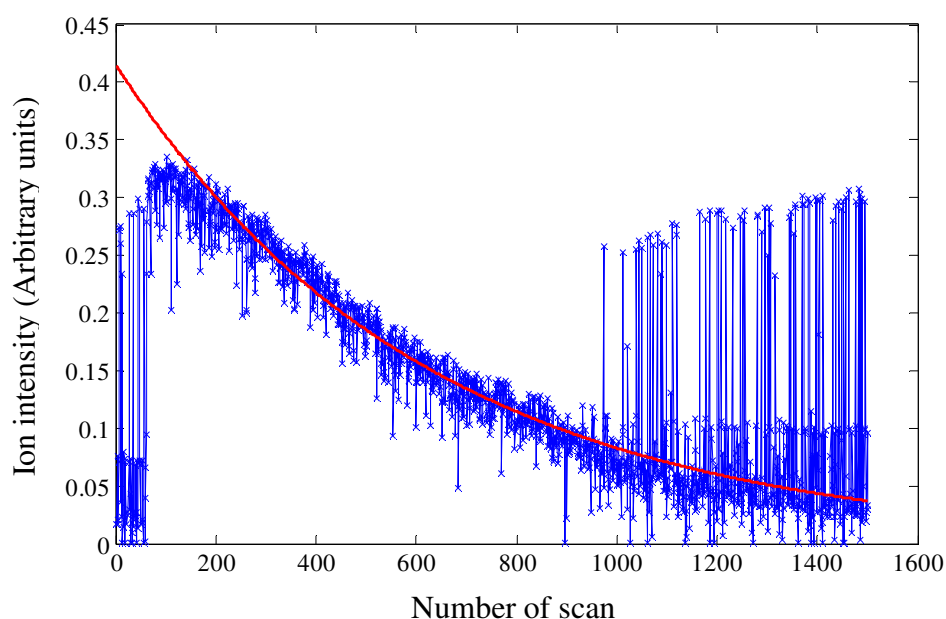


**Figure H.11** Raw data (blue) plotted alongside fitted exponential (red)

It is important to assess the range that the exponential fit is relevant. In order to achieve this, the natural log of the amended data is plotted against a curve fit of higher order of the same data. The result of this is displayed within Figure H.12. This gives a graphical representation of where the assumption of an exponential decrease of signal is valid.

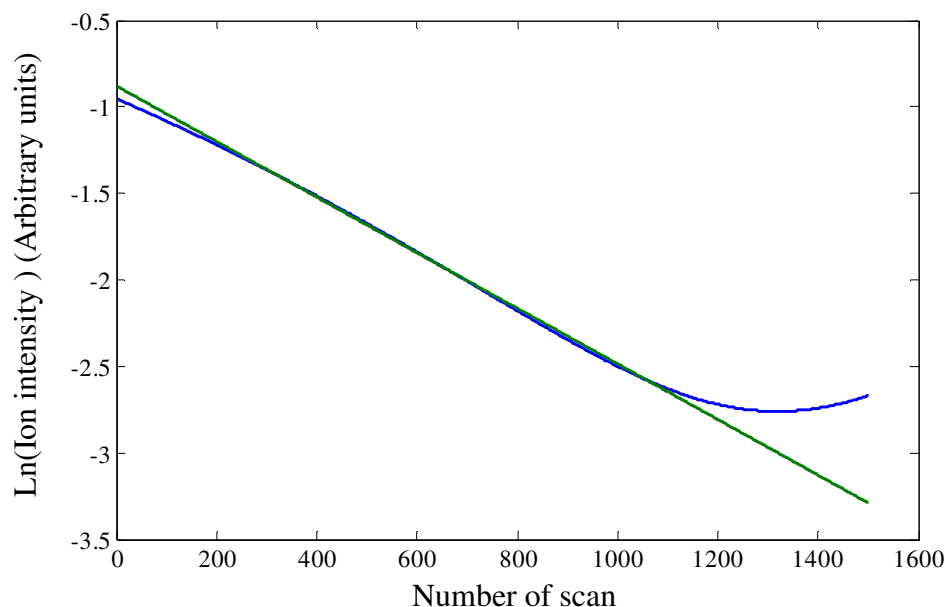


**Figure H.12** Line of best fit of the logarithm of the amended data (green) and a higher order curve fit of the curve fit (blue)

Inspecting Figure H.12 the two lines are in good agreement with one another between a Number of Scan range of 250 to 1075. Beyond these two values it appears that the fitted exponential no longer provides a good representation of the raw data and the assumption of a purely exponential decrease is incorrect. The limits stated above also appear to correlate with where the fitted exponential is in poor agreement with the raw data as observed from Figure H.11.

This indicates the limits of where the exponential decrease is valid and can be used to calculate a limit of detection. All this was only possible because of the peak fitting that was undertaken. The recorded information enabled isolation of the most relevant data which

could then be used to further focus on a mathematical expression for the exponential dilution.

## **H.VI Summary**

Originally the data set had a great deal of incorrectly fitted data which corresponded to several separate CV values. A user defined range was utilised so that only data with a suitable CV value was used for further analysis. Since some data had been disregarded replacement data was required and the result was used to discover constants which described, in a mathematical expression, the exponential decrease of ion intensity.

---

## **APPENDIX I: Ion velocity and displacement with respect to $E/N$**

---

In Chapter 5 a constant  $E/N$  environment was maintained by adjusting the electric field strength and pressure of carrier flow within the FAIMS sensor. An alternative way of explaining what is being undertaken is to consider the velocity of a single ion within an idealised ion swarm.

The ion accelerates in accordance with its unique mobility within the applied electric field. When the ion collides with a neutral constituent of the carrier flow its velocity is assumed to be completely lost. The ions velocity then again increases in the same manner until it experiences another collision. The velocity which the ion can accomplish determines its displacement within the separation of the waveform and is therefore representative of the observed compensation voltage of the ion swarm.

Assuming the ion experiences a constant acceleration between collisions an arbitrary velocity profile can be formulated. Following this, the displacement of the ion within the separation region can also be calculated. With this simple model modifying the electric field strength (which affects the acceleration of the ion) and pressure of carrier flow (which changes the frequency of collisions) can be visualised. Figure I.1 shows the velocity and displacement of two ions.

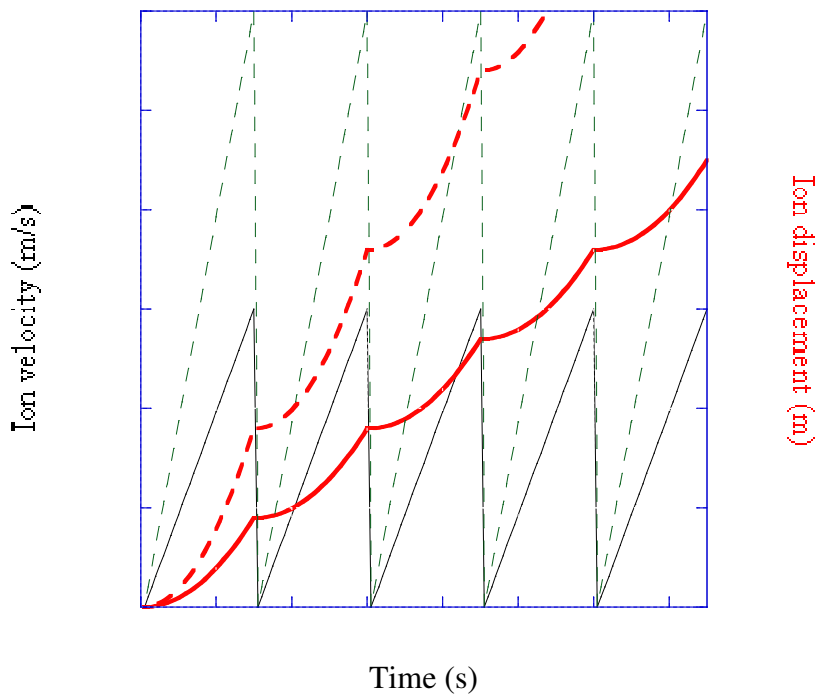


**Figure I.1** The velocity and displacement of two ions are described. The velocity and displacement of the first ion described by the solid black line and solid red line respectively. The velocity and displacement of the second ion is described by the dashed green and dashed red line respectively.

The pressure experienced by both ions in Figure I.1 is the same as represented by an identical frequency of collisions. The electric field strength experienced by the second ion is, however, twice the magnitude of that experienced by the first ion. It can be seen that the conditions of higher electric field have resulted in an increase in the distance travelled per unit time.

Figure I.2 describes two ions which experience the same electric field strength but the second ion is in a carrier flow with a pressure twice that of the first ion.

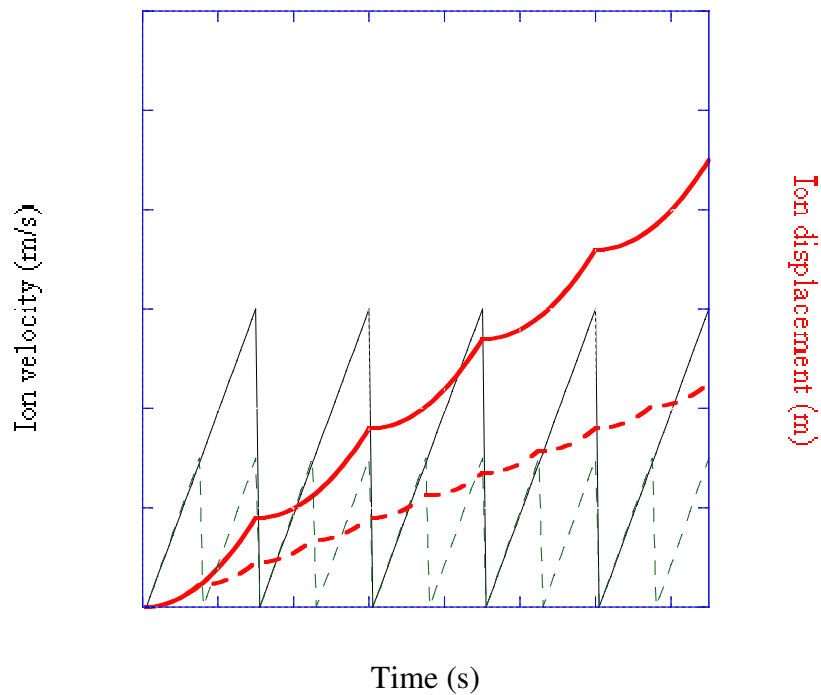


**Figure I.2** The velocity and displacement of two ions are described. The velocity and displacement of the first ion is described by the solid black line and solid red line respectively. The velocity and displacement of the second ion is described by the dashed green and dashed red line respectively.

This time the second ion has a smaller displacement per unit time compared to the first ion.

This is because while the acceleration experienced by the two ions is identical the second ion undergoes more collisions so its average acceleration, following its first collision, is less than the first ion.

In Figure I.3 the electric field and pressure imposed on the first ion are identical as the two previous cases. The magnitude of the electric field and pressure of carrier flow imposed on the second ion are now both twice that for the first ion.

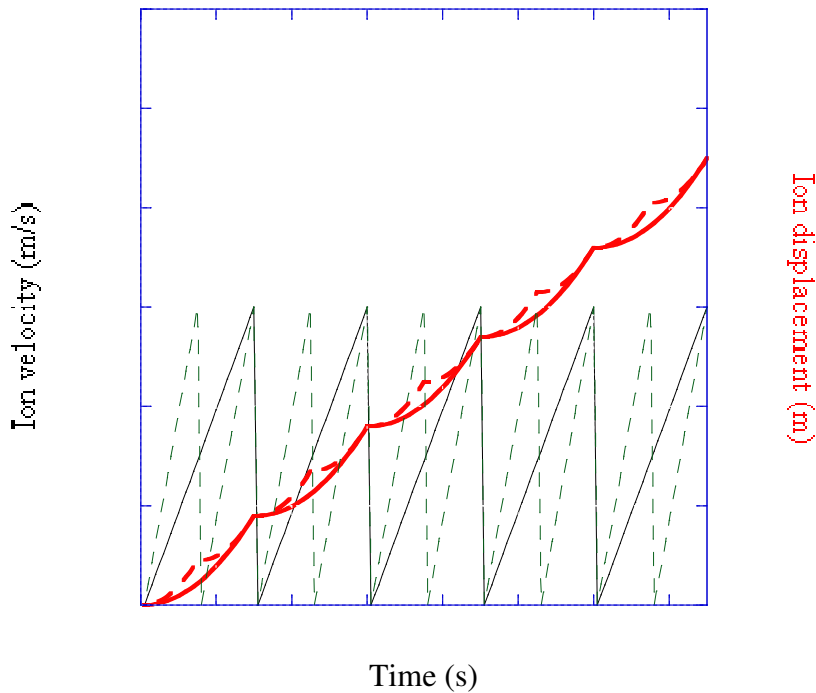


**Figure I.3** The velocity and displacement of two ions are described. The velocity and displacement of the first ion is described by the solid black line and solid red line respectively. The velocity and displacement of the second ion is described by the dashed green and dashed red line respectively.

Since the effects of electric field and pressure are linear upon the ion velocity the two conditions result in a consistent displacement per unit time of the ions. Despite the change in conditions it is the ratio  $E/P$  (therefore also  $E/N$ ) which is important. It is this methodology which has been employed to ensure the  $E/N$  environments, despite a variation in carrier flow pressure, can be maintained so that it is possible to better understand the effects of varying the pressure and electric field strength imposed.

It is important to be aware that the plots presented here are not linked to the asymmetric waveform, other than to the magnitude of the electric field imposed. Ions will interact with a huge number of neutral constituents within a single period of the applied waveform at all the pressures studied.

## Appendix references

1. Krylova, N., Krylov, E., Eiceman, G.A., and Stone, J.A., *Effect of moisture on the field dependence of mobility for gas-phase ions of organophosphorus compounds at atmospheric pressure with field asymmetric ion mobility spectrometry*. Journal of Physical Chemistry A, 2003. **107**(19): p. 3648-3654.
2. Eiceman, G.A. and Karpas, Z., *Ion Mobility Spectrometry*. Second ed. 2005: Taylor & Francis. 350.
3. Mohammad, A., *ANALYTE MOISTURE CHEMISTRY IN FIELD ASYMMETRIC IMS*. 2007: ISIMS 2007, Mikkeli, Finland.
4. Shvartsburg, A.A., *Differential Ion Mobility Spectrometry*. 2009, Boca Raton: CRC Press, Taylor and Francis Group.
5. Krylov, E.V. and Nazarov, E.G., *Electric field dependence of the ion mobility*. International Journal of Mass Spectrometry, 2009. **285**: p. 149 -156.
6. McDaniel, E.W. and Mason, E.A., *The Mobility and Diffusion of Ions in Gases*. 1973: Wiley. 372.
7. Mason, E.A. and McDaniel, E.W., *Transport Properties of Ions in Gases*. 1988: Wiley, New York.
8. Nazarov, E.G., Coy, S.L., Krylov, E.V., Miller, R.A., and Eiceman, G.A., *Pressure effects in differential mobility spectrometry*. Analytical Chemistry, 2006. **78**(22): p. 7697-7706.
9. Shvartsburg, A.A., Smith, R.D., Wilks, A., Koehl, A., Ruiz-Alonso, D., and Boyle, B., *Ultrafast Differential Ion Mobility Spectrometry at Extreme Electric Fields in Multichannel Microchips*. Analytical Chemistry, 2009. **81**(15): p. 6489–6495.
10. Hastie, T., Tibshirani, R., and Friedman, J., *The Elements of Statistical Learning*. 2001: Springer.

